Efficiency improvements of silicon solar cells by the impurity photovoltaic effect

M. J. Keevers and M. A. Green
Centre for Photovoltaic Devices and Systems, University of New South Wales, P.O. Box 1, Kensington NSW 2033, Australia

(Received 2 August 1993; accepted for publication 18 November 1993)

A theoretical investigation of the impurity photovoltaic (IPV) effect for improving silicon solar-cell efficiency is presented. The approach is better than previous analyses because of the improved treatment of generation and recombination via impurities, and because it includes the effects of optical competition and light trapping. The approach is applied to the nonmidgap, deep-level impurity indium as the IPV effect impurity incorporated into an idealized silicon solar cell. The analysis is based on experimentally determined parameters for indium. Improvements of cell current, subgap spectral response, and energy conversion efficiency are quantified. The analysis reveals the importance of light trapping and proper selection of indium and dopant concentrations. The impurity photovoltaic effect is predicted to improve solar-cell efficiency.

I. INTRODUCTION

It is possible to improve solar-cell performance by taking advantage of subgap absorption processes to increase the long-wavelength response. One approach is to deliberately incorporate impurities (or more generally, defects) into the device to allow carrier generation via impurity levels, the impurity photovoltaic (IPV) effect (Fig. 1). In 1960, Wolf[1] suggested this effect could significantly improve efficiencies of solar cells by increasing current output. A criticism was voiced by Shockley and Queisser,[2] who argued that efficiency improvements would be improbable because the improved carrier generation would be at the expense of increased recombination in the cell. This was later confirmed for midgap impurities by Güttler and Queisser.[3] Their analysis showed that while midgap impurities would be most favorable, incorporating such impurities into silicon solar cells would not improve efficiency. A recent calculation by Würfel[4] of the detailed-balance limit of the efficiency of silicon solar cells incorporating a midgap defect further supports the conclusion that midgap levels are not promising in this regard. Recent experimental work by Li *et al.*[5] on a novel silicon structure purports to show that dramatic efficiency improvements are possible with the defect photovoltaic effect. These authors attributed the improvement to a thin layer of defects deliberately incorporated into their cell near the *p-n* junction. They claim to have achieved an efficiency of 35%. This claim has received considerable interest. Unfortunately, it is rather doubtful, as evidenced by the many objections raised.[6] In fact, those making the 35% efficiency claim have since acknowledged that "the work was not perfectly done."[7]

Here we reevaluate the potential of the IPV effect for increasing solar-cell efficiency. The study was originally motivated by the recognition that light trapping significantly enhances the potential of the IPV effect, due to the improved long-wavelength absorption. Our approach is new in three respects: (i) A formulation of impurity effects is employed which includes both the recombinative and the photogenerative role the impurity can play; (ii) account is taken of competing absorption processes; and (iii) the effect of light trapping is included. The approach can be utilized in solar-cell simulations, or simpler analyses, to investigate the IPV effect in solar cells. Specifically, we consider the nonmidgap, deep-level impurity indium as the IPV effect impurity incorporated into an idealized silicon solar cell. We calculate the increase of the cell's light-generated current, long-wavelength spectral response, and efficiency due to the indium incorporation. This article is the full version of work presented in condensed form at the 23rd IEEE Photovoltaics Specialists Conference.[8]

II. THEORY

A. Modified Shockley–Read–Hall recombination model

Our analysis is based upon a modified Shockley–Read–Hall (SRH) model for recombination via impurities (or more generally, defects). In the standard SRH model, electrons and holes can be captured by the impurity, and thermally excited from it. The modified model includes the two impurity optical transitions of Fig. 1. The six impurity-related transitions included in the modified SRH model are shown in Fig. 2.

For steady-state conditions, the net recombination rate U via an impurity level is given by[9,10]

$$U=\frac{np-n_1^*p_1^*}{\tau_{n0}(p+p_1^*)+\tau_{p0}(n+n_1^*)}, \tag{1}$$

where

$$\tau_{n0}=1/c_nN_t, \quad \tau_{p0}=1/c_pN_t, \tag{2}$$

$$n_1^*=n_1+\tau_{n0}g_{n,\max}, \quad p_1^*=p_1+\tau_{p0}g_{p,\max}, \tag{3}$$

$$n_1=g_tN_ce^{-(E_c-E_t)/kT}, \quad p_1=\frac{1}{g_t}N_ve^{-(E_t-E_v)/kT}, \tag{4}$$

$$g_{n,\max}=N_t\int_{\lambda_g}^{\lambda_{n,\max}}2\sigma_n^{\mathrm{opt}}(\lambda)\phi_{\mathrm{ph}}(x,\lambda)d\lambda, \tag{5a}$$

 0021-8979/94/75(8)/4022/10/$6.00 © 1994 American Institute of Physics

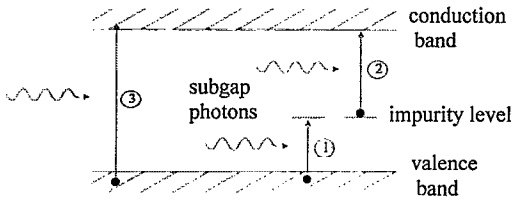

FIG. 1. The IPV effect: Subgap photons create electron-hole pairs via impurity levels (1 and 2). Compare to intrinsic band-to-band absorption (3).

$$g_{p,\max}=N_t\int_{\lambda_g}^{\lambda_{p,\max}} 2\sigma_p^{\text{opt}}(\lambda)\phi_{\text{ph}}(x,\lambda)\,d\lambda, \tag{5b}$$

with the occupancy of the impurity level given by[11]

$$f_t=\frac{c_n n N_t+c_p p_1 N_t+g_{p,\max}}{c_n N_t(n+n_1)+(g_{n,\max}+g_{p,\max})+c_p N_t(p+p_1)}. \tag{6}$$

Equation (1) is widely applicable, nondegeneracy being the major assumption. n and p are the electron and hole concentrations, τ_{n0} and τ_{p0} are the SRH low-injection lifetimes for electrons and holes, N_t is the impurity concentration, c_n and c_p are the electron and hole capture coefficients, g_t is the impurity-level degeneracy factor and E_t the impurity-level energy, E_c and E_v are the conduction and valence-band edges, and N_c and N_v are the effective densities of states in the conduction and valence bands [$N_c=2.86\times10^{19}$ cm^{-3}, $N_v=3.10\times10^{19}$ cm^{-3} (Ref. 12)].

The terms most crucial to the present analysis are the optical generation terms $g_{n,\max}$ and $g_{p,\max}$ [Eqs. (5a) and (5b)]. $g_{n,\max}$ is the optical emission rate of electrons from the impurity (process 2 of Fig. 1), with the impurity fully occupied. $g_{p,\max}$ is the optical emission rate of holes from the impurity (process 1 of Fig. 1), with the impurity completely empty. $\sigma_n^{\text{opt}}(\lambda)$ and $\sigma_p^{\text{opt}}(\lambda)$ are the electron and hole photoemission cross sections of the impurity, with thresholds at $\lambda_{n,\max}$ and $\lambda_{p,\max}$, respectively. The lower limit on the wavelength integrations is assumed to be the silicon bandgap wavelength $\lambda_g=1.107$ μm. We assume that all shorter-wavelength photons are utilized by intrinsic band-to-band absorption (process 3 of Fig. 1). $\phi_{\text{ph}}(x,\lambda)$ is the photon flux density at a distance x from the illuminated front surface. The factor 2 is a geometrical factor to account for the oblique passage of light within the textured cell considered (Sec. II C).

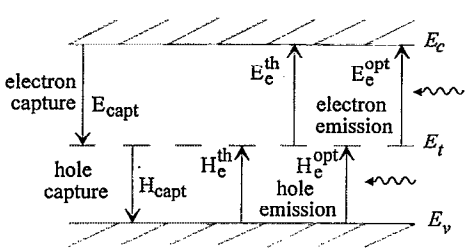

FIG. 2. The six transitions of the modified SRH recombination model. Electron and hole emission can occur thermally (th) or optically (opt).

TABLE I. Indium parameters (at 300 K) used in this study.[a]

Indium property	Symbol	Value /model
Energy level	E_t	$E_v+0.157$ eV[b]
Degeneracy factor	g_t	4[c]
Hole capture coeff. (negative charged In)	c_p	8×10^{-8} cm^3 s^{-1} [d]
Electron capture coeff. (neutral In)	c_n	2×10^{-15} cm^3 s^{-1} [e]
Hole photoemission cross section	$\sigma_p^{\text{opt}}(\lambda)$	Edwards–Fowler theory[f] (fitted to a max.[g] of 0.5×10^{-16} cm^2)
Electron photoemission cross section	$\sigma_n^{\text{opt}}(\lambda)$	two models[h] (see Fig. 3)

[a]Reference 10.
[b]Reference 13.
[c]See Refs. 14 and 15.
[d]Reference 16.
[e]References 17–19.
[f]References 20 and 21.
[g]Reference 22.
[h]Reference 23 (and Refs. 17 and 24).

One reason that our analysis of the IPV effect in solar cells is an improvement on earlier ones is because it is based on the modified SRH expression of Eq. (1). This equation treats the impurity in a self-contained way. U is either positive or negative, indicating that, as far as the SRH recombination mechanism is concerned, the impurity acts solely either to increase recombination (i.e., to decrease carrier lifetimes) or to increase photogeneration in the cell.

The basic idea of the present article is that for some impurities incorporated into a solar cell, the recombination rate U in Eq. (1) may be negative, indicating improved current generation. The inclusion of the photoemission terms [Eq. (5)] is central to this. Moreover, by including the effects of light trapping, the balance is shifted in favor of a given impurity providing such a net generation.

B. Choice of impurity

Electron-hole pair creation via an impurity is a two-step process. Thus, a midgap impurity will maximize the amount of the subgap spectrum that is accessible to the IPV effect [Eq. (5)], however, *e-h* pair creation will then rely on two weak optical processes. On the other hand, a shallow impurity provides much less access to the subgap spectrum, but it allows one of the excitation processes to be strong, as it occurs thermally. This leaves only one of the two steps dependent on weak optical excitation. A non-midgap but deep-level impurity is a compromise which provides both reasonable access to the subgap spectrum, and reliance on only one of the weak impurity optical processes. We have chosen the deep acceptor indium, which produces an energy level 157 meV (Ref. 13) above the valence-band edge.

The relevant properties of indium in silicon at 300 K have been reviewed,[10] and are summarized in Table I. The values for n_1 and p_1 are 6.4×10^3 and 1.8×10^{16} cm^{-3} [Eq. (4)]. The magnitude of p_1 indicates that for indium in silicon, hole emission from the indium level is overwhelm-

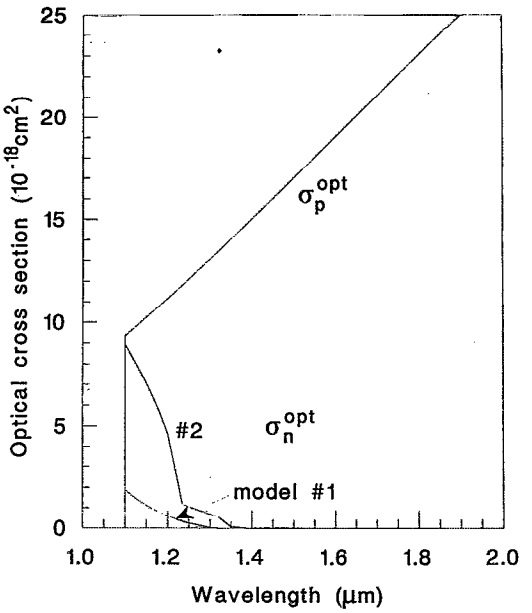

FIG. 3. Optical cross sections σ_n^{opt} and σ_p^{opt} of indium in silicon in the wavelength range of interest. Two models are used for σ_n^{opt}, providing upper and lower bounds.

ingly thermal and not optical. The smallness of n_1 indicates that the electron photoemission term $g_{n,\max}$ [Eq. (5a)] is crucial if U is to be negative [$n_1^* p_1^* \approx p_1 \tau_{n0} g_{n,\max}$ in Eq. (1)]. Electron photoemission from indium, being the slower of the two excitation processes, is the rate-limiting step. Thus, for indium in silicon, absorption of photons by the hole photoemission process only provides competition to the crucial electron photoemission process. Due to the paucity of experimental data available for σ_n^{opt} (which is needed to calculate $g_{n,\max}$), we consider two different models of this parameter (Fig. 3). Model no. 1 is based on low-temperature impurity photoconductivity measurements,[24] while model no. 2 is based on low-temperature photoluminescence measurements (to determine c_n) and detailed-balance theory.[17] Figure 3 shows that σ_p^{opt} increases with increasing wavelength (σ_p^{opt} peaks at 4 μm and has a threshold at 8 μm), while σ_n^{opt} decreases. Both the electron and hole optical cross sections are assumed zero for above-gap photons.

C. Idealized solar cell

Consider the 300-μm-thick crystalline silicon solar cell of Fig. 4. It is assumed to be operating under global AM1.5 illumination[25] (96.4 mW/cm^2) and a temperature of 300 K. We focus on the base region because subgap absorption processes are relatively weak and the base constitutes most of the cell volume. The base region can contain both a shallow (and therefore fully ionized) background dopant, as well as the IPV impurity indium. The amount of background dopant is described by $N_{b,\mathrm{sh}}$, the net shallow donor concentration, which can be positive (n type), negative (p type), or zero. The indium concentration is described by N_t. We consider $N_{b,\mathrm{sh}}$ and N_t to be present in the starting

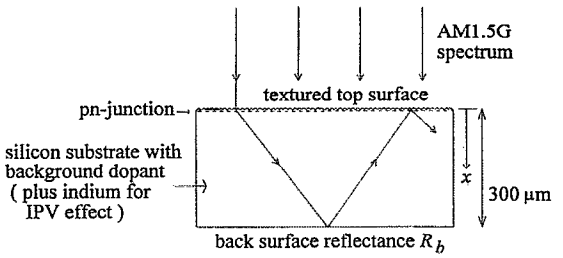

FIG. 4. The silicon solar cell under investigation.

wafers (introduced at the crystal-growth stage, for example), and both to be spatially uniform. The occupancy f_t of the indium level is given by Eq. (6). Both the background dopant $N_{b,\mathrm{sh}}$ and the indium N_t (if present) determine the effective doping of the base region ($N_{b,\mathrm{eff}} = N_{b,\mathrm{sh}} - f_t N_t$).

The nonequilibrium carrier concentrations in the base are determined by the condition of space-charge neutrality, i.e.,

$$p - n + N_{b,\mathrm{sh}} - f_t N_t = 0. \tag{7}$$

In order to relate n and p in a simple way we consider the case of an idealized cell with perfect surface passivation, base diffusion length much larger than the cell thickness, and infinite carrier mobilities. With these assumptions, the n-p product throughout the device can be approximated by[9]

$$np = n_i^2 e^{qV/kT}. \tag{8}$$

V is the cell voltage, and n_i the intrinsic carrier concentration [$n_i = 1.07 \times 10^{10}$ cm^{-3} (Ref. 12)]. It also follows from these idealizations that all photogenerated minority carriers are collected by the p-n junction.

The cell has a randomizing top surface with a perfect antireflection (AR) coating, and a planar back surface of reflectivity R_b. This structure brings about light trapping for weakly absorbed light. The degree of light trapping is adjusted by the parameter R_b. Light trapping effectively enhances the photon flux inside the cell. By considering the path described by the mean Lambertian light ray, the following expression[10] is obtained for the internal photon flux of Eq. (5):

$$\phi_{\mathrm{ph}}(x,\lambda) = \frac{1 + e^{-4\alpha_{\mathrm{tot}}(\lambda)(W-x)} R_b}{1 - e^{-4\alpha_{\mathrm{tot}}(\lambda) W} R_t R_b} e^{-2\alpha_{\mathrm{tot}}(\lambda) x} \phi_{\mathrm{ext}}(\lambda). \tag{9}$$

$\phi_{\mathrm{ext}}(\lambda)$ is the incident AM1.5G spectrum. The absorption coefficient α_{tot} includes all absorption processes in the cell:

$$\alpha_{\mathrm{tot}}(\lambda) = \alpha_n(\lambda) + \alpha_p(\lambda) + \alpha_{\mathrm{fc}}(\lambda) + \alpha_{e\text{-}h}(\lambda), \tag{10}$$

where

$$\alpha_n(\lambda) = f_t N_t \sigma_n^{\mathrm{opt}}(\lambda), \tag{11}$$

$$\alpha_p(\lambda) = (1 - f_t) N_t \sigma_p^{\mathrm{opt}}(\lambda), \tag{12}$$

$$\alpha_{\mathrm{fc}}(\lambda) = (2.7 \times 10^{-18} p + 1.8 \times 10^{-18} n) \lambda^2. \tag{13}$$

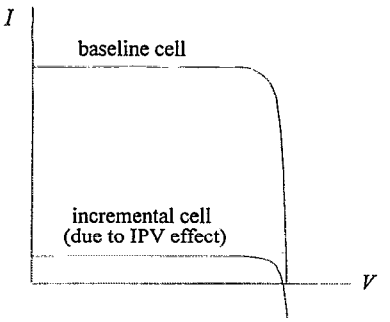

FIG. 5. The superposition approach.

α_n is the absorption coefficient for electron photoemission from the IPV impurity (process 2 of Fig. 1), and α_p represents hole photoemission from the IPV impurity (process 1 of Fig. 1). α_{fc} is the absorption coefficient for free-carrier absorption,[26] a process which does not result in the creation of electron-hole pairs. $\alpha_{e\text{-}h}$ is the absorption coefficient for intrinsic band-to-band e-h pair creation (process 3 of Fig. 1). α_{tot} in the form of Eq. (10) accounts for competition between the four absorption processes.

D. Superposition approach

We use a superposition approach[9] to evaluate performance boosts due to indium's IPV effect. This involves considering the cell to be composed of two solar cells in parallel, each with its own I-V curve (Fig. 5). One cell is the unperturbed baseline cell containing no indium. The second, incremental cell accounts for the subgap photocurrent due to incorporation of indium. The total cell output after indium incorporation is found by adding the baseline and incremental I-V curves.

Three issues arise from the indium incorporation as follows.

(i) To account for the fact that indium in silicon competes for subgap photons that might otherwise contribute, however weakly, to the current derived from intrinsic band-to-band absorption, a correction is made to the incremental cell current.

(ii) Indium acts as a dopant. Before indium is incorporated, the effective base doping is equal to the background donor concentration, i.e., $N_{b,\text{eff }0} = N_{b,\text{sh }0}$ (where 0 denotes the initial value). With indium, we will consider two conceptually simple possibilities: (a) the background dopant concentration remains fixed at its initial value, $N_{b,\text{sh}} = N_{b,\text{sh }0}$, enabling the effective doping $N_{b,\text{eff}}$ to change; and (b) the effective doping remains fixed at its initial value $N_{b,\text{eff}} = N_{b,\text{eff }0}$ by adjustment to $N_{b,\text{sh}}$.

(iii) We neglect any impact of increased dopant concentration on material quality.

E. Photocurrent improvement

The increase of photocurrent due to the IPV impurity is

$$J_{L,\text{IPV}} = J_{L,\text{bare IPV}} + \Delta J_{e\text{-}h}, \tag{14}$$

where

$$J_{L,\text{bare IPV}} = q\int_0^W [-U(x)]\,dx, \tag{15}$$

$$\Delta J_{e\text{-}h} = J_{e\text{-}h,\text{ with In}} - J_{e\text{-}h,\text{ no In}}. \tag{16}$$

$J_{L,\text{bare IPV}}$ is the current increase due to indium acting as a modified SRH recombination center. If U is negative, $J_{L,\text{bare IPV}}$ is positive and indium acts as a generation center. $\Delta J_{e\text{-}h}$ is the (negative) correction term described in Sec. II D.

To a good approximation for indium in silicon at 300 K, f_t [Eq. (6)] and U [Eq. (1)] are given by

$$f_t = p_1/(p+p_1), \tag{17}$$

$$U = (1-f_t)c_n n N_t - f_t g_{n,\max} = E_{\text{capt}} - E_e^{\text{opt}}. \tag{18}$$

At room temperature, the indium occupancy is essentially determined by hole thermal emission H_e^{th} and hole capture H_{capt} (Fig. 2). Equation (18) indicates that the electron processes E_e^{opt} and E_{capt} (Fig. 2) are the rate-determining steps for e-h pair creation and recombination via indium, respectively. Neglecting the extremely weak x dependence of p and n introduced by the x dependence of the subgap photon flux $\phi_{\text{ph}}(x,\lambda)$ [Eq. (9)], we perform the x integration in Eq. (15) for $J_{L,\text{bare IPV}}$ to obtain

$$J_{L,\text{bare IPV}} = q\int_{\lambda_g}^{\lambda_{n,\max}} \frac{\alpha_n(\lambda)}{\alpha_{\text{tot}}(\lambda)} a_{\text{LT}}(\lambda)\phi_{\text{ext}}(\lambda)\,d\lambda - \frac{qnpW}{\tau_{n0}(p+p_1)}, \tag{19}$$

where

$$a_{\text{LT}}(\lambda) = \frac{\int_0^W 2\alpha_{\text{tot}}(\lambda)\phi_{\text{ph}}(x,\lambda)\,dx}{\phi_{\text{ext}}(\lambda)} = \frac{(1+e^{-2\alpha_{\text{tot}}(\lambda)W}R_b)(1-e^{-2\alpha_{\text{tot}}(\lambda)W})}{1-e^{-4\alpha_{\text{tot}}(\lambda)W}R_tR_b}. \tag{20}$$

a_{LT} is the total absorbance of the cell, i.e., the fraction of incoming light at a particular wavelength that is absorbed in the cell by any of the four processes in α_{tot} [Eq. (10)]. $(\alpha_n/\alpha_{\text{tot}})\,a_{\text{LT}}$ is the absorbance for the crucial rate-limiting electron photoemission process.

The correction term $\Delta J_{e\text{-}h}$ is calculated from the difference of two terms [Eq. (16)]. Both $J_{e\text{-}h,\text{ no In}}$ and $J_{e\text{-}h,\text{ with In}}$ represent the contribution to the photocurrent from subgap photons and the subgap tail of $\alpha_{e\text{-}h}$. $J_{e\text{-}h,\text{ no In}}$ is calculated with no IPV impurity present, and $J_{e\text{-}h,\text{ with In}}$ is calculated with the IPV impurity present. They are given by

$$J_{e\text{-}h,\text{ with In}} = q\int_{\lambda_g}^{\lambda_{\max}} \frac{\alpha_{e\text{-}h}(\lambda)}{\alpha_{\text{tot}}(\lambda)} a_{\text{LT}}(\lambda)\phi_{\text{ext}}(\lambda)\,d\lambda, \tag{21}$$

$$J_{e\text{-}h,\text{ no In}} = q\int_{\lambda_g}^{\lambda_{\max}} \frac{\alpha_{e\text{-}h}(\lambda)}{\alpha'_{\text{tot}}(\lambda)} a'_{\text{LT}}(\lambda)\phi_{\text{ext}}(\lambda)\,d\lambda. \tag{22}$$

The primes in Eq. (22) indicate that the two IPV absorption processes (α_n and α_p) are absent, and n and p are determined without the IPV impurity present.

F. Energy conversion efficiency and subgap spectral response

The subgap spectral response of the solar cell is calculated under short-circuit conditions, with AM1.5G light[25] bias. The response for the cell without indium is determined by calculating the incremental change to $J_{e\text{-}h,\ \text{no In}}$ [Eq. (22)] due to incrementing the AM1.5G spectrum separately at each wavelength. The response for the cell with indium present is determined by calculating the incremental changes to $J_{L,\text{bare IPV}}+J_{e\text{-}h,\ \text{with In}}$ [Eqs. (15) and (21)].

To evaluate the efficiency increase due to the IPV effect we use the superposition approach of Sec. II D. The baseline cell is the cell of Fig. 4 without indium. This cell has a short-circuit current density of 43 mA/cm^2, due to intrinsic band-to-band absorption. We consider its open-circuit voltage to be between 700 and 760 mV. In the Auger limit, its open-circuit voltage would be about 755 mV.[9] The baseline cell is modeled using these parameters and a simple one-diode model equation, with an ideality factor of one. These parameters yield a baseline cell efficiency between 26.4% and 29.0%, depending on the open-circuit voltage assumed. After indium incorporation, the new maximum power point of the combined cells (baseline plus incremental) is determined. The new efficiency is then compared to the baseline cell efficiency, in order to determine any improvements due to indium.

III. RESULTS AND DISCUSSION

A. Short-circuit current improvement

When indium acts as a generation center (U negative), to a high degree of accuracy the rate of electron-hole pair creation is simply the rate for electron photoemission, i.e.,

$$E_e^{\text{opt}} = -U = f_t N_t \int_{\lambda_g}^{\lambda_{n,\max}} 2\sigma_n^{\text{opt}} \phi_{\text{ph}}\, d\lambda. \tag{23}$$

The threshold wavelength for electron photoemission is between 1.32 and 1.38 μm (Fig. 3), depending on the σ_n^{opt} model. If all subgap photons in the AM1.5G spectrum of shorter wavelength were absorbed by this process, then the short-circuit current would increase by 6–8.5 mA/cm^2. This indicates that indium has considerable access to the subgap spectrum.

1. Indium incorporation for fixed background dopant concentration

First, we examine whether indium can improve the short-circuit current without significantly altering the base doping. To do so, we consider the conceptually simple case of incorporating indium into a cell with a fixed background dopant concentration. Figure 6 shows the dependence of the incremental short-circuit current $J_{\text{sc,IPV}}$ on indium concentration. The shallow background dopant is n type, with a concentration of $N_{b,\text{sh}} = 10^{17}$ cm^{-3}. The figure also shows the effect of the optical correction term (which accounts

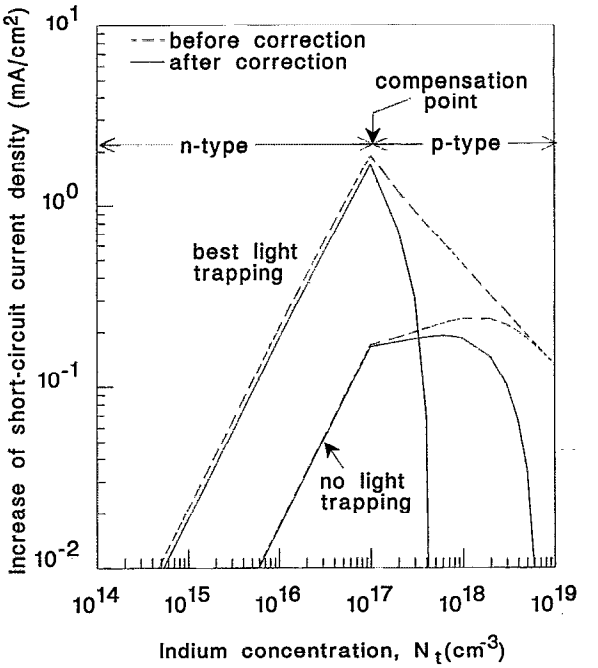

FIG. 6. Short-circuit current improvement as a function of indium concentration for a fixed background donor concentration of 10^{17} cm^{-3}. The effect of light trapping and the correction term of Eq. (14) is included. Model no. 2 for σ_n^{opt} is assumed.

for the competition indium presents to subgap intrinsic absorption) and the importance of light trapping. The dashed curves show $J_{\text{sc,bare IPV}}$ [Eq. (15) with $V=0$], which neglects the correction term. The solid curves show the final IPV effect current improvement after correction, $J_{\text{sc,IPV}}$ [Eq. (14) with $V=0$]. No light trapping refers to a rear reflectivity R_b of zero, and best light trapping refers to perfect rear reflectivity $R_b=1$ (which is the best light trapping under the randomizing scheme).

Significant current improvement ($\sim$1 mA/cm^2) does occur for the best light trapping case, but only in the region where indium compensates the background n-type dopant. Without light trapping the current does show improvement, however, it is not substantial. For indium concentrations that undercompensate the background dopant, the indium level is fully occupied [$p \ll p_1$, Eq. (17)]. As expected from Eq. (23), the current then increases linearly with indium concentration. When indium overcompensates the n-type dopant, the indium level is not fully occupied. This allows subgap photons to be absorbed by the noncrucial hole photoemission process, which reduces the photon flux ϕ_{ph} available for the crucial electron process [Eq. (23)]. Such competition between the two indium optical processes accounts for the decline of the uncorrected current boost (dashed curves) at high indium concentrations. The even more dramatic decline at high indium concentrations seen after the correction term is included (solid curves) indicates that hole photoemission also competes significantly with subgap intrinsic absorption.

What is the effect of different background dopant types? Fig. 7 shows the incremental short-circuit current as a function of indium concentration for various background

dopants. The best results occur for n-type background dopants (solid curves), and the more heavily n type the better. The undoped case performs worse than the n-type dopant, and the p-type dopant case (dashed curve) yields the smallest current improvement. For all cases the trends with indium concentration are qualitatively very similar, although the peaks are considerably sharper in the n-type case. The reason for the same trends lies in the indium level occupancy, Eq. (17). For hole concentrations well below the value p_1, the occupancy is essentially a constant with increasing indium concentration, and the current boost increases linearly also [Eq. (23)]. When the indium doping is sufficient to make the hole concentration comparable to or larger than p_1, the indium occupancy decreases, thus enabling the competitive action of the hole photoemission process to take effect. The reason that an n-type shallow dopant enables indium to provide a better IPV effect current boost is that it keeps the indium level fully occupied, thus suppressing the effect of competition from the noncrucial hole photoemission process.

Significant improvements only occur when indium is at least close to compensating the background n-type dopant. Then the indium does alter the effective doping of the base. This is not compatible with a cell designed to have a certain base doping concentration (without indium). It is conceptually better then to consider indium incorporation, and at the same time adjustment of the background dopant concentration, so that the effective base doping is kept constant.

2. Indium incorporation for constant effective base doping

Figure 8 shows the short-circuit current improvement as a function of indium concentration for perfect compensation of the background doping density. Best light trapping is assumed, and two models of the electron photoemission cross section are considered. Without the indium the cell bulk is undoped. This case is relevant to the intrinsic region of p-i-n solar cells and, for example, to Stanford University's Backside-Contact solar cells.[27] Indium incorporation is considered in conjunction with shallow n-type dopant incorporation so that the effective doping of the bulk remains zero. At an indium doping of 10^{17} cm^{-3} the current boost is small but not insignificant (up to 1.5 mA/cm^2). This indium concentration seems compatible with the assumption of negligible material degradation, although indium doping may result in lower lifetimes than the same concentration of the usual p-type dopant boron.[28] At the indium solubility limit of 10^{18} cm^{-3},[29] significant current boosts occur for both electron photoemission models (2 and 5 mA/cm^2, respectively). These are not necessarily ruled out by material quality considerations. There is evidence that compensated material suffers less lifetime degradation than uncompensated material with the same dopant concentration.[30] In fact, in the Auger limit, compensation will improve carrier lifetimes because of the reduced carrier concentrations. Figure 8 also indicates that, beyond the solubility limit, the short-circuit current improves further with increasing (compensated) indium concentrations. If one considers very high indium concentrations (not shown in the figure), there is actually a saturation of the current boost at about 6 or 8.5 mA/cm^2 (depending on the model). These values correspond to extending the cell's subgap response to 100% at the threshold wavelength for electron photoemission (see the beginning of Sec. III A).

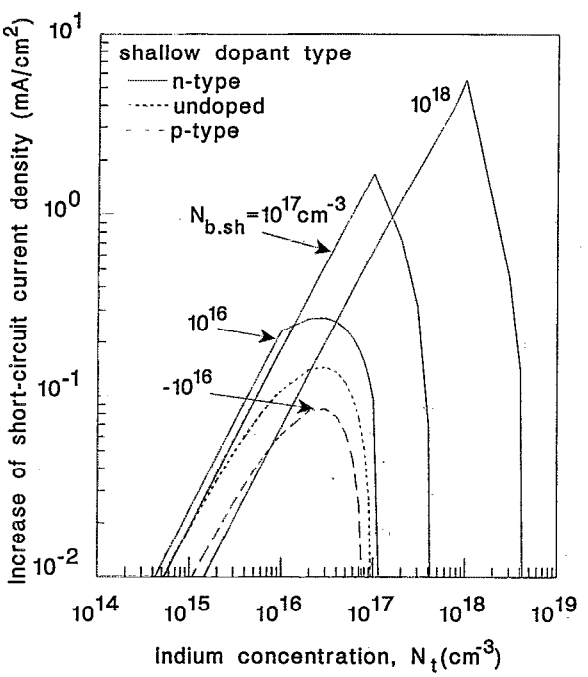

FIG. 7. Short-circuit current improvement as a function of indium concentration for various background dopants. Best light trapping and model no. 2 for σ_n^{opt} are assumed.

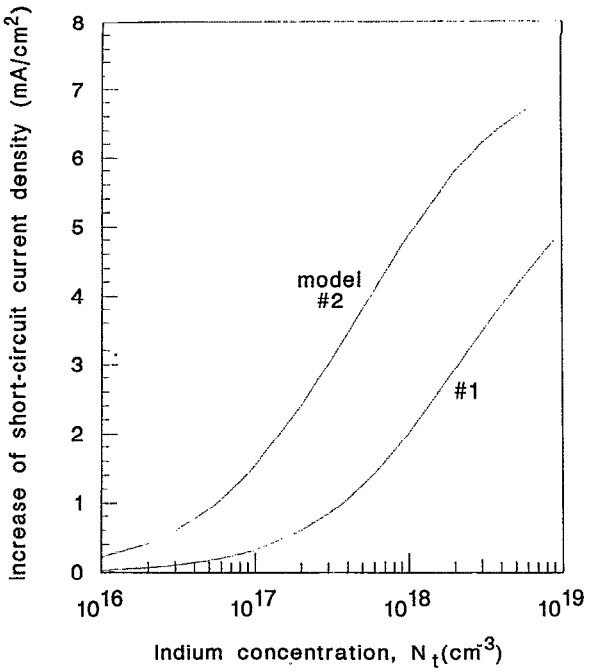

FIG. 8. Short-circuit current improvement for a perfectly compensated base region. Best light trapping is assumed, and both models for σ_n^{opt} are considered.

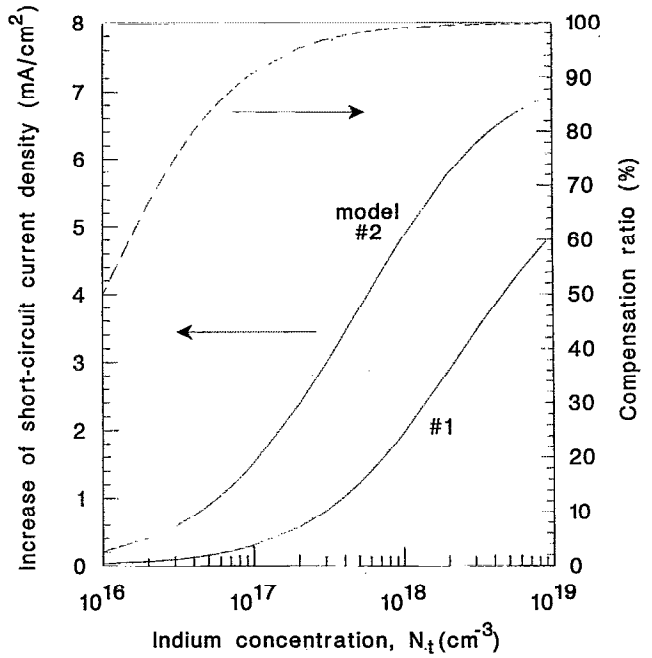

FIG. 9. Short-circuit current improvement as a function of indium concentration, for the case of indium slightly undercompensating the n-type background dopant (effective base doping is maintained at 10^{16} cm^{-3} n type). Best light trapping, and both models for σ_n^{opt} considered. The extent to which indium compensates the n-type background dopant is also shown.

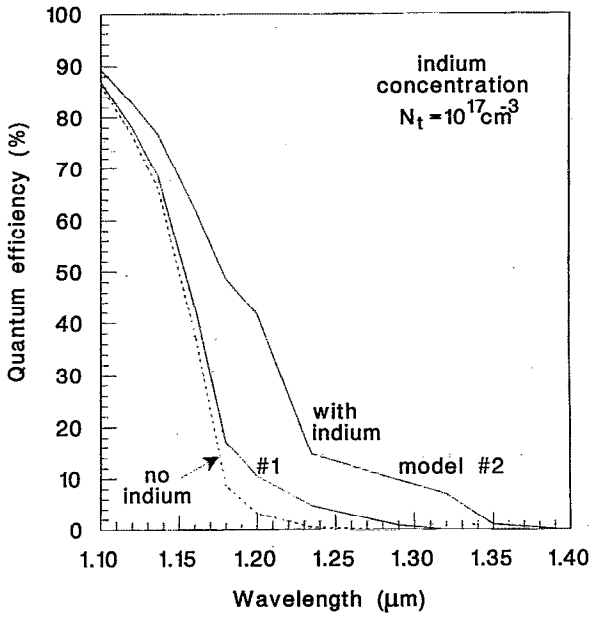

FIG. 10. Effect of indium incorporation on subgap spectral response. The same case as in Fig. 9 is considered, with an indium concentration of $N_t = 10^{17}$ cm^{-3} (indium 91% compensates the background n-type dopant).

Figure 9 shows the short-circuit current improvement as a function of indium concentration when indium slightly undercompensates the background n-type dopant. The results are quantitatively very similar to those of Fig. 8 for the perfectly compensated case. For each indium concentration, the background dopant concentration is adjusted so that the effective base doping is n type at 1×10^{16} cm^{-3}. For example, when indium is incorporated to a concentration of 10^{17} cm^{-3}, it is considered to occur in conjunction with incorporation of n-type dopant to a concentration of 1.1×10^{17} cm^{-3}, resulting in an effective base doping of 1×10^{16} cm^{-3}. The indium then compensates 91% of the background dopant. For an indium concentration of 10^{18} cm^{-3}, and with the same effective doping, the indium needs to compensate 99% of the background dopant. When indium slightly undercompensates the background dopant as in Fig. 9, the benefits of a fully occupied indium level (see Sec. III A 1) remain.

Having an n-type base region rather than the conventional p-type base does not present a problem. The effective base doping of 1×10^{16} cm^{-3} n type is relevant to the high-efficiency n-type PERL (passivated emitter, rear locally diffused) cells of UNSW.[31] These cells satisfy, or are approaching, some of the assumptions employed in our analysis. PERL cells exhibit very good light trapping, have diffusion lengths much larger than the cell width, and have excellent surface passivation. The assumption of infinite mobility is discussed below. The neglect of material quality degradation resulting from indium incorporation (and background dopant adjustment) may not be too severe. This was discussed above. Near (or perfect) compensation between high levels of indium and the shallow donor impurity may be obtained by, for example, neutron transmutation of silicon to form phosphorus.[32] This technique has been used to precisely compensate residual acceptors in indium-doped infrared detector material.[33] Thus, a good fraction of the short-circuit current improvements shown in Fig. 9, in particular for indium concentrations up to around 10^{17} cm^{-3}, are likely to be experimentally accessible with the PERL structure.

B. Subgap spectral response

Subgap spectral response measurements are an effective tool to experimentally assess the IPV role of an impurity. Figure 10 compares the subgap spectral response of our ideal solar cell before and after indium incorporation. Figure 10 is calculated for the same undercompensated case as in Fig. 9, with an indium concentration of 10^{17} cm^{-3} (and a shallow n-type dopant concentration of 1.1×10^{17} cm^{-3}). The cell without indium has an n-type dopant concentration of 10^{16} cm^{-3}. Figure 10 shows that indium incorporation in this manner improves the subgap spectral response for all subgap wavelengths, and in particular between 1.15 and 1.35 μm. Figure 10 indicates that measurements of the subgap spectral response of silicon solar cells with optimized indium incorporation may help determine more accurate values for the electron photoemission cross section for indium in silicon, a parameter which at present has a paucity of experimental data. The dashed curve of Fig. 10 shows that for wavelengths up to

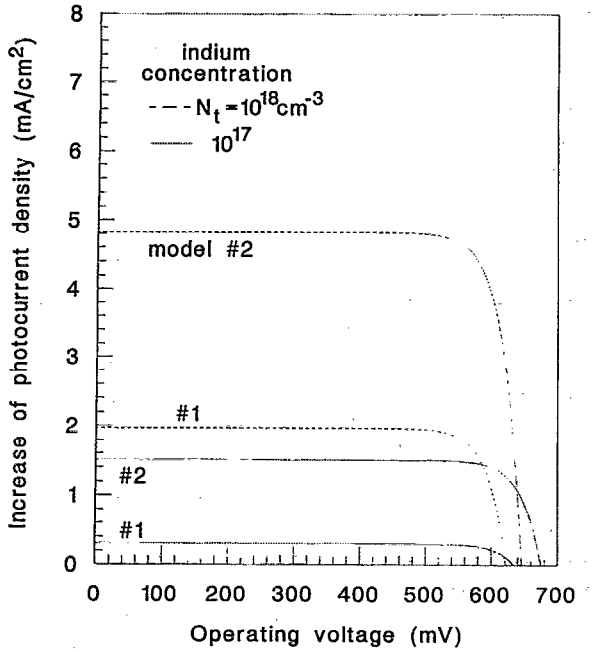

FIG. 11. Voltage dependence of the IPV light-generated current. The same case as in Fig. 9 is considered, with indium concentrations of 10^{17} (solid lines) and 10^{18} cm^{-3} (dashed lines), corresponding to 91% and 99% compensation.

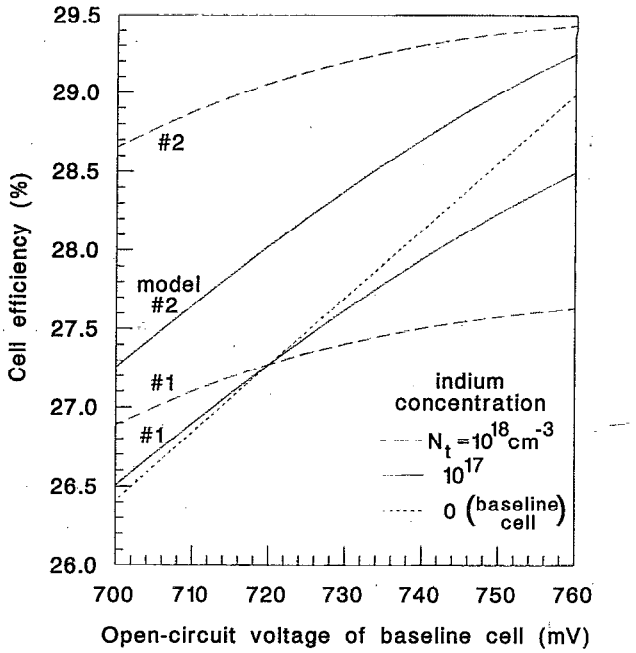

FIG. 12. Cell efficiency after indium incorporation, as a function of baseline cell open-circuit voltage, for the cases considered in Fig. 11. Indium concentration 10^{17} (solid lines) and 10^{18} cm^{-3} (large-dashed lines), effective base doping n type 10^{16} cm^{-3}, best light trapping, and two models for σ_n^{opt}. The efficiency of the baseline cell (which has no indium) is also shown for comparison (small-dashed line).

about 1.15 μm, the response due to intrinsic band-to-band absorption dominates. This justifies use of the correction term, Eq. (16).

C. Efficiency improvements

The investigation of short-circuit current conditions (Sec. III A) has allowed us to determine optimal doping conditions. It was shown that significant current improvements can occur. For efficiency improvements to occur, the IPV effect must remain beneficial at nonzero voltages. Figure 11 shows the effect of operating voltage on the IPV light-generated current calculated from Eq. (14). Two different indium concentrations are considered for the same conditions as in Fig. 9, i.e., best light trapping is assumed and an effective doping of 10^{16} cm^{-3} is maintained. Note that light trapping is important, not only because it significantly enhances the current improvement, but also because it maintains that improvement for higher voltages. The curves are flat up to moderate voltages due to the dominance of indium's generative role over its recombinative role. As the voltage is increased further, the free-carrier concentrations increase to such values that recombination through the indium level becomes significant [Eqs. (8) and (19)]. Eventually, p and n become sufficiently large that impurity recombination matches IPV generation and there is no current boost. This occurs between 600 and 700 mV, for the cases considered in Fig. 11. For higher voltages, the incremental current rapidly becomes large and negative (in other words, the modified SRH recombination rate U [Eq. (1)] becomes positive). Therefore, overall cell current output is reduced. Since the baseline cell has an open-circuit voltage between 700 and 760 mV, indium incorporation reduces open-circuit voltage.

Before considering any effects on cell efficiency, we want to discuss the infinite mobility assumption. The simple expression for the n-p product [Eq. (8)] introduces the voltage dependence into the IPV photocurrent. It relies on the limiting assumption of infinite carrier mobilities. At short circuit, $V=0$ and Eq. (8) grossly underestimates the n-p product for real cells under illumination. For example, at short circuit under one-sun illumination, PERL cells have minority-carrier concentrations of about 5×10^{13} cm^{-3}. Combined with a majority-carrier concentration of 10^{16} cm^{-3}, this yields an n-p product of 5×10^{29} cm^{-3}. To obtain these magnitudes from Eq. (8), one has to consider that $V\approx580$ mV. We see from Fig. 11 that the IPV photocurrent at 580 mV is only marginally below its $V=0$ value. At the maximum power point and open-circuit voltage of PERL cells (600 and 700 mV, respectively) Eq. (8) is a reasonable approximation. Thus, the infinite mobility assumption is not so extreme as to rule out application of the results here to real cells. In order to properly model the IPV effect in actual solar cells, however, full solar-cell simulations need to be carried out. This could be done, for example, by using an appropriately modified version of PC1-D.[34]

Figure 12 shows the improvement indium's IPV effect yields to the absolute efficiency of the ideal solar cell, as a function of the baseline cell's open-circuit voltage. The efficiency of the baseline cell (small-dashed line), which has no indium, varies between 26.4% and 29.0% as its open-

circuit voltage varies from 700 to 760 mV. For the cases shown, the baseline cell efficiency is generally improved upon by the IPV effect of indium. The same cases as in Fig. 11 are considered, that is, best light trapping, indium concentrations of 10^{17} (solid lines) and 10^{18} cm^{-3} (large-dashed lines), effective base doping of 10^{16} cm^{-3}, and two models for the electron photoemission cross section. For each baseline cell open-circuit voltage, the superposition approach described in Sec. II D was employed. Each I-V curve of Fig. 11 was added to the I-V curve for the baseline cell, and the new maximum power point and hence efficiency were determined. As seen above, indium incorporation leads to significant short-circuit current improvements in some cases. However, it reduces cell open-circuit voltage since the current improvement is not maintained up to sufficiently large operating voltages relative to the baseline cell open-circuit voltage (above 700 mV, Fig. 11). When the short-circuit current improvement outweighs the open-circuit voltage reduction, there is an efficiency increase.

Figure 12 shows that indium incorporation does give significant efficiency improvements for some baseline cells. Present high-efficiency n-type PERL cells have open-circuit voltages of about 700 mV. According to Fig. 12, for an indium incorporation of 10^{17} cm^{-3} (with a similar amount of n-type dopant), the absolute efficiency improves by between 0.1% and 0.8% for this baseline V_{oc}. For an indium incorporation of 10^{18} cm^{-3}, the efficiency improves by between 0.5% and 2.2%, for this baseline V_{oc}. Figure 12 also shows that efficiency improvements are smaller for larger baseline cell open-circuit voltages. This occurs because the larger the baseline cell open-circuit voltage, the larger is the reduction in open-circuit voltage resulting from indium incorporation. This larger open-circuit voltage reduction then detracts more from the benefit of improved short-circuit current, leading to smaller efficiency boosts. However, even for limiting baseline open-circuit voltages (about 755 mV), the open-circuit voltage reduction does not outweigh the short-circuit current improvement (at least for the upper bound σ_n^{opt} model). In this case, for the two indium concentrations considered, the efficiency improves by 0.3% to 0.6% absolute. Thus, even though poorer baseline cells show larger IPV effect improvement, the impurity photovoltaic effect is capable of extending solar-cell efficiency limits. Other IPV impurities may fare even better than our choice of indium.

IV. CONCLUSIONS

This work presents an improved analysis of the IPV effect in silicon solar cells. The approach is based on a modified Shockley–Read–Hall model for recombination via impurities, which includes the photogenerative role of the impurity. This is an improvement on previous analyses because it treats generation and recombination via impurities together. Furthermore, our approach incorporates the effects of light trapping. This is important because light trapping shifts the balance in favor of a given impurity providing a net generation. We also take account of optical competition between the impurity processes, intrinsic band-to-band absorption, and free-carrier absorption. Our approach is quite general and can be used to investigate IPV effect performance improvements in solar cells for any promising candidate impurity.

General arguments relevant to the selection of a favorable IPV impurity lead to our choice of the nonmidgap, but deep-level impurity indium. The approach is applied to indium as the IPV impurity incorporated into an ideal silicon solar cell. The calculations are based on reported experimental parameters for indium in silicon. The rate-limiting step for electron-hole pair creation via indium is the electron photoemission process, since hole emission is strong and provided thermally. We use two models to represent upper and lower bounds on the electron photoemission cross section. The solar cell considered is assumed electronically ideal in that it has long diffusion lengths, perfect surface passivation, and infinite carrier mobilities. Optically, it has a randomizing light trapping scheme and can have perfect rear reflectivity. Our calculations therefore represent upper limits for the IPV improvements of indium. However, the results are also related, with qualification, to present high-efficiency silicon solar cells. In future, improved analysis of the IPV effect in real solar cells could be achieved using a solar-cell simulation that utilizes the approach presented here.

Our work reveals the importance of light trapping and the need to have indium approximately compensated by an n-type dopant. Light trapping significantly enhances the IPV effect current boost, and it maintains that boost for higher operating voltages. Compensating the indium keeps it fully occupied. This keeps the rate-determining electron photoemission process supplied with bound electrons, suppresses recombination via the indium level, and suppresses absorption of photons by the noncrucial hole photoemission process. If the latter process is not minimized, it competes not only with the electron photoemission from the indium, but also with electron-hole pair creation by intrinsic band-to-band absorption.

Our calculations show that significant short-circuit current improvements (up to 5 mA/cm^2) result from indium incorporation, provided there is good light trapping, the indium concentration is at least about 10^{17} cm^{-3}, and the indium is close to compensation by an n-type dopant. Spectral response calculations confirm that such improvements are due to extension of the long-wavelength response into the sub-bandgap region, and they also indicate that spectral response measurements are able to improve experimental data on the optical cross section for photoemission from the indium level. Indium incorporation, even under the most favorable conditions, reduces the open-circuit voltage of our model cell because of indium's role as a recombination center at high operating voltages. However, such reductions are outweighed by the improvements of the cell short-circuit current. Indium incorporation indeed significantly improves cell energy conversion efficiency, by as much as 1%–2% absolute. This is the first time that the impurity photovoltaic effect is predicted to improve solar-cell efficiency.

ACKNOWLEDGMENTS

This work is partly supported by the Australian Research Council and the Energy Research and Development Corporation. The Centre for Photovoltaic Devices and Systems is funded by the Australian Research Council's Special Research Centres Scheme and by Pacific Power. The authors would like to thank members of the Centre for their helpful discussions.

[1] M. Wolf, Proc. IRE **48**, 1246 (1960).
[2] W. Shockley and H. J. Queisser, J. Appl. Phys. **32**, 510 (1961).
[3] G. Güttler and H. J. Queisser, Energy Convers. **10**, 51 (1970).
[4] P. Würfel, Sol. Energy Mater. Sol. Cells **29**, 403 (1993).
[5] J. Li, M. Chong, J. Zhu, Y. Li, J. Xu, P. Wang, Z. Shang, Z. Yang, R. Zhu, and X. Cao, Appl. Phys. Lett. **60**, 2240 (1992).
[6] E. Demesmaeker, M. Ghannam, J. Nijs, R. Mertens, R. Van Overstraeten, H. A. Aulich, R. Wieting, M. Rodot, and J. C. Müller, Appl. Phys. Lett. **63**, 849 (1993); J. Gee and S. R. Wenham, Tutorial Notebook, 23rd IEEE Photovoltaic Specialists Conference, Louisville, KY, May 1993, p. 32; M. A. Green, Semicond. Sci. Technol. **8**, 1 (1993); A. Luque, Appl. Phys. Lett. **63**, 848 (1993); Sol. Energy Mater. Sol. Cells **29**, 415 (1993); A. Morales-Acevedo, Appl. Phys. Lett. **63**, 850 (1993); A. Rohatgi, E. R. Weber, and L. C. Kimerling, J. Electron Mater. **22**, 65 (1993); C. Summonte, M. Biavati, E. Gabilli, R. Galloni, S. Guerri, R. Rizzoli, and F. Zignani, Appl. Phys. Lett. **63**, 785 (1993); C. Summonte, F. Corticelli, R. Lotti, P. Negrini, A. Poggi, Q. Zini, and F. Zignani, in Proceedings of the 11th European Communities Photovoltaic Solar Energy Conference, Montreux, Switzerland, Oct. 1992, p. 370; and Ref. 4.
[7] J. Li, M. Chong, J. Zhu, Y. Li, J. Xu, P. Wang, Z. Shang, Z. Yang, R. Zhu, and X. Cao, Appl. Phys. Lett. **63**, 851 (1993).
[8] M. J. Keevers and M. A. Green, in Conference Record of the 23rd IEEE Photovoltaic Specialists Conference, Louisville, KY, May 1993.
[9] M. A. Green, *High Efficiency Silicon Solar Cells* (Trans. Tech., Aedermannsdorf, 1987).
[10] M. J. Keevers and M. A. Green, Internal Report (1992/01), Centre for Photovoltaic Devices and Systems, UNSW, June 1992.
[11] Y. K. Hsieh and H. C. Card, J. Appl. Phys. **65**, 2409 (1989).
[12] M. A. Green, J. Appl. Phys. **67**, 2944 (1990).
[13] *Landolt-Bornstein: Numerical Data and Functional Relationships in Science and Technology, New Series III/22b*, edited by M. Schulz (Springer, Berlin, 1990).
[14] K. Geim, G. Pensl, and M. Schulz, Appl. Phys. A **27**, 71 (1982).
[15] G. J. Parker, S. D. Brotherton, I. Gale, and A. Gill, J. Appl. Phys. **54**, 3926 (1983).
[16] Calculated from the value 5×10^{-7} cm^3 s^{-1} at 50 K of Ref. 14, by including the degeneracy factor $g_t=4$, and by adjusting to a 300 K value assuming a $T^{-1.8}$ temperature dependence.
[17] B. O. Sundstrom, L. Huldt, and N. G. Nilsson, J. Phys. C **15**, 3359 (1982).
[18] B. O. Sundstrom, L. Huldt, and N. G. Nilsson, Solid State Commun. **17**, 787 (1975); Phys. Scr. **18**, 413 (1978).
[19] Note that the value for c_n obtained by Sundstrom and co-workers in Refs. 17 and 18 supports the low values reported earlier by Y. E. Pokrovskii and K. I. Svistunova, Phys. Status Solidi **33**, 517 (1969).
[20] A. H. Edwards and W. B. Fowler, Phys. Rev. B **16**, 3613 (1977).
[21] Note that W. Schelter, W. Hell, R. Helbig, and M. Schulz, J. Phys. C **15**, 5839 (1982) have shown that the Edwards–Fowler theory (Ref. 20) gives a better fit to the experimental data than does the Lucovsky model [G. Lucovsky, Solid State Commun. **3**, 299 (1965)]. This is important so that competition to the crucial σ_n^{opt} process from the high-energy tail of σ_p^{opt} is not overestimated.
[22] This value for the maximum σ_p^{opt} (which occurs at 4 μm) is half of the low-temperature value 1×10^{-16} cm^2 [which is the average of the low-temperature values obtained by Schelter *et al.* (see Ref. 21) and Parker *et al.* (Ref. 15)], to account for the decrease of σ_p^{opt} with increasing the temperature to 300 K.
[23] The two models for σ_n^{opt}, models no. 1 and no. 2, are based on the low-temperature measurements of Chikovani and Pokrovskii (Ref. 24) and Sundstrom and co-workers (Ref. 17), respectively, and are shifted by 50 meV to lower energies to adjust to 300 K values.
[24] R. I. Chikovani and Y. E. Pokrovskii, Sov. Phys. Solid State **8**, 1856 (1967).
[25] R. Hulstrom, R. Bird, and C. Riordan, Sol. Cells **15**, 365 (1985).
[26] D. K. Schroder, R. N. Thomas, and J. C. Swartz, IEEE Trans. Electron Devices **ED-25**, 254 (1978).
[27] R. A. Sinton, R. R. King, and R. M. Swanson, in Proceedings of the 4th International Photovoltaic Science and Engineering Conference, Sydney, Australia, 1989, p. 143.
[28] T. F. Ciszek, T. Wang, T. Schuyler, and A. Rohatgi, J. Electrochem. Soc. **136**, 230 (1989).
[29] H. M. Hobgood, T. T. Braggins, M. M. Sopira, J. C. Swartz, and R. N. Thomas, IEEE Trans. Electron Devices **ED-27**, 14 (1980).
[30] D. Margadonna, F. Ferrazza, and R. Peruzzi, in Proceedings of the 10th European Photovoltaic Solar Energy Conference, Lisbon, Portugal, 1991, p. 678.
[31] X. M. Dai, M. A. Green, and S. R. Wenham, in Conference Record of the 23rd IEEE Photovoltaic Specialists Conference, Louisville, KY, May 1993.
[32] Suggested to M. A. G. by P. A. Iles of Applied Solar Energy Corporation, 1993.
[33] R. N. Thomas, T. T. Braggins, H. M. Hobgood, and W. J. Takei, J. Appl. Phys. **49**, 2811 (1978); T. T. Braggins, H. M. Hobgood, J. C. Swartz, and R. N. Thomas, IEEE Trans. Electron Devices **ED-27**, 2 (1980); H. M. Hobgood, T. T. Braggins, M. M. Sopira, J. C. Swartz, and R. N. Thomas, *ibid.* **ED-27**, 14 (1980).
[34] P. A. Basore, in Conference Record of the 22nd IEEE Photovoltaic Specialists Conference, Las Vegas, NV, October 1991, p. 299.